Simulation study of type-II Ge/Si quantum dot for solar cell applications

Weiguo Hu, Mohammad Maksudur Rahman, Ming-Yi Lee, Yiming Li, and Seiji Samukawa

Articles you may be interested in

Ge/Si quantum dots thin film solar cells
Appl. Phys. Lett. **103**, 082101 (2013); 10.1063/1.4818999

Simulation of charge carriers generation rate of SiGe quantum dot based intermediate band solar cell
AIP Conf. Proc. **1454**, 203 (2012); 10.1063/1.4730721

Carrier transport and sensitivity issues in heterojunction with intrinsic thin layer solar cells on N-type crystalline silicon: A computer simulation study
J. Appl. Phys. **107**, 054521 (2010); 10.1063/1.3326945

Origin of the optical gap dependence of a- SiGe solar cell stability
J. Appl. Phys. **84**, 4611 (1998); 10.1063/1.368687

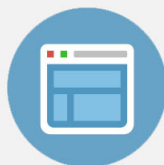a- SiGe:H based solar cells with graded absorption layer
J. Appl. Phys. **84**, 611 (1998); 10.1063/1.368088

Simulation study of type-II Ge/Si quantum dot for solar cell applications

Weiguo Hu,[1,2] Mohammad Maksudur Rahman,[1,2] Ming-Yi Lee,[3] Yiming Li,[3,4,a)] and Seiji Samukawa[1,2,4,b)]

[1]*Institute of Fluid Science, Tohoku University, Sendai 980-8577, Japan*
[2]*Japan Science and Technology Agency, CREST, Tokyo 102-0075, Japan*
[3]*Department of Electrical and Computer Engineering, National Chiao Tung University, Hsinchu 300, Taiwan*
[4]*WPI Advanced Institute for Materials Research, Tohoku University, Sendai 980-8577, Japan*

The electronic structure, miniband formation conditions, and required process parameters of type-II Ge/Si quantum dots are calculated using a 3D finite element method. We further estimate the device conversion efficiency and optimize the appropriate operation conditions. By using the crystalline silicon as the matrix, the explored intermediate band solar cell (IBSC) may not be suitable for 1 sun application, but it is a great value under concentration application. By considering an appropriate H-passivation treatment on amorphous silicon, the type II Ge/Si IBSC can achieve 44.0% conversion efficiency under 1 sun application. © 2013 AIP Publishing LLC. [http://dx.doi.org/10.1063/1.4821114]

Thanks to the large element abundance and well-developed semiconductor process, silicon-based solar cell has larger than 85% market share. However, due to the Shockley-Queisser (S-Q) limit, its conversion efficiency still stops at 25%, which may not satisfy diverse commercial application.[1] Intermediate band solar cell (IBSC) proposed by Luque *et al.* has become a promising candidate for breaking the S-Q limitation.[2,3] The prototype cells have been fabricated with mature InAs/GaAs quantum dot (QD). Device core mechanism, two-photon-transition, has been reported with various experiments.[4,5] One of the next significant issues will be the structure design optimization for real-world energy device's application. Silicon-based solar cells have been of great interest; however, growth of silicon-based QD may face process difficulties such as, a precise size control due to a small Bohr radius, a high order alignment for miniband formation, a complex indirect band structure, and a kinetic growth limitation. Recently, Kechiantz *et al.* has analysed the band alignment between Si/Ge heterojunction and indicated the possibility of intermediate band solar cell.[6] However, their works have not yet touched the concrete quantum effect with experiment or theory yet. In addition, a clear prediction on the conversion efficiency is still lack.

In this article, a 3D finite element method (FEM) is developed to calculate the electronic structure of type-II Ge/Si QDs which could be fabricated by our top-down nanotechnology. We study the miniband formation conditions and required process parameters for the type Ge/Si IBSC. Notably, by solving the classical detailed balance model, we further estimate the device conversion efficiency and optimize the appropriate operation conditions.

By combining the self-assemble bio-template and damage-free neutral beam etching (NBE), we apply the top-down process to fabricate sub-10 nm uniform and well aligned type-II Si/Ge QDs superlattice. The fabrication process is illustrated in Figs. 1(a)–1(d); this nanofabrication technique can first control the QD thickness by the deposition thickness and its diameter by the bio-template, which brings the higher flexibility on engineering quantum levels. Second, thanks to stable DNA duplicate, the QD superlattice keeps a high uniformity and quasi-crystalline in-plane alignment. At the same time, the ideal vertical alignment is achieved with one-step etching on stacked Ge/Si layers. Third, the regrowth process is independent with the etching process, which indicates various possible matrix materials. Figure 1(e) shows the etched Ge/Si nanopillars before regrowth matrix, which exhibits a good uniformity and alignment. With further process parameters, we can achieve same ideal QD superlattices which are similar to our recent work in the silicon system.[7] In this study, we mainly focus on the 3D FEM simulation and design of the type-II Ge/Si QDs IBSC. The electronic structure is numerically solved on the basis of envelope-function approximation,[8]

$$\left(-\frac{\hbar^2}{2m^*}\nabla^2 + V\right)\psi = E\psi, \qquad (1)$$

where $\hbar$, m^*, V, E, ψ are the reduced Planck's constant, the effective mass, the position-dependent potential energy, the quantum levels, and the electron envelope function, respectively. The adopted parameters are listed in Table I. Under the light illumination, excessive carriers split the quasi fermi levels to generate photovoltage,[3,9–12]

$$V = \mu_{VC} = Ef_C - Ef_V, \qquad (2)$$

where the μ_{VC} is the the chemical potential, f_c and f_v are quasi-fermi levels of conduction band and valence band, respectively. In the IBSC, the electron density is described by[3,9–12]

$$\frac{dn}{dt} = (G_{VC} - R_{VC}) + (G_{IC} - R_{IC}) + \frac{1}{q}\frac{dJ_n}{dx}, \qquad (3)$$

a)E-mail: ymli@faculty.nctu.edu.tw
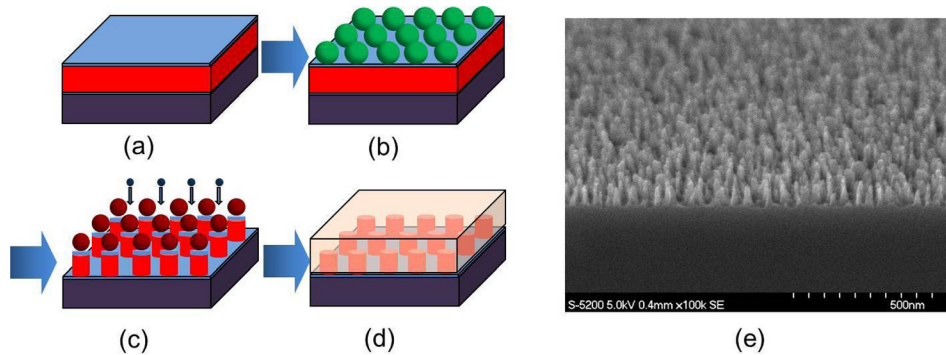b)E-mail: samukawa@ifs.tohoku.ac.jp

FIG. 1. (a) Ge/Si stacked layers deposition; (b) ferritin self-assemble; (c) damage-free neutral beam etching; (d) matrix regrowth; (e) Ge/Si nanopillars before regrowth matrix.

TABLE I. Parameters used for the simulation of type-II Ge/Si QDs.

	Si	Ge
Electron effective mass	0.36 m_0 (Ref. 17)	0.22 m_0 (Ref. 18)
Heavy hole effective mass	0.49 m_0 (Ref. 19)	0.28 m_0 (Ref. 19)
Light hole effective mass	0.16 m_0 (Ref. 20)	0.044 m_0 (Ref. 21)
Bandgap	1.12 eV (Ref. 6)	0.66 eV (Ref. 6)
Conduction band-offset	0.05 eV (Ref. 6)	
Valence band-offset	0.51 eV (Ref. 6)	

where n is the electron density, t is the time (For the solar cell works under the equilibrium state, the left term of Eq. (3) is vanished.), x is the spatial position along light incident, J_n is the photo current, q is electron charge, G is the carrier generation rate, and R is recombination rate. The recombination rate depends on the photovoltage. Finally, the current-voltage (I-V) profile is deduced from Eqs. (2) and (3) accordingly.

The proposal type-II Ge/Si QDs IBSC device and operation process are shown in Fig. 2. The Ge QD is embedded into the silicon matrix, which acts as the absorbing layer of IBSC. The built-in field is induced with the p-n junction. This structure is very similar to the traditional Silicon-based solar cell; and therefore, it can be easily integrated into fabrication process. For the IBSC applications, the type-II Ge/Si QD has two great advantages: (i) their band-offset mainly lies on one of the bands, the band-offset in the valence band (VB) is 0.51 eV and that the conduction band (CB) is only 0.05 eV. It means that electron can freely transport and hole

is pumped out of potential well to get high mobility. This is very near to the ideal IBSC design.[3] (ii) The core interband/intraband transitions in the Ge/Si QD have been widely used with various materials and devices.

The prediction of IBSC operation is the intermediate band formation. By using the 3D FEM, we calculate the energy band of the hexagonal alignment type II Ge/Si QD superlattice, where the diameter and thickness are 6.4 nm and 4 nm, respectively. Note when the quantum dots are closely well aligned, their wavefunctions diffuse into and couple with each other, which form quasi-continuous minibands. The interdot space determines the coupling strength. Figure 3 shows the miniband's structure of the type II Ge/Si QD superlattice with respect to various interdot spaces. As shown in Fig. 5, both the two light hole induced minibands and the three heavy hole induced minibands appear below the valence edge. Due to the small effective mass, the light hole induced minibands have wider bandwidth and easily couple with heavy hole's excited states. Ideally, the intermediate band should be separated from continuous valence band or conduction band with zero-density-state to inhibit rapid phonon relaxation process. Some experiments and theories reveal that the phonon bottle-neck effects alleviate this relaxation.[12,13] However, this mechanism has not been studied in the type II Ge/Si QDs. Consequently, we incline to follow the strict IBSC concept. The ground state of heavy hole keeps a far larger than thermal energy gap between any minibands, which can be chosen as a proper intermediate band. With increasing interdot space from 0.5 nm to 4 nm, the ground sate minibands width exponentially decrease from
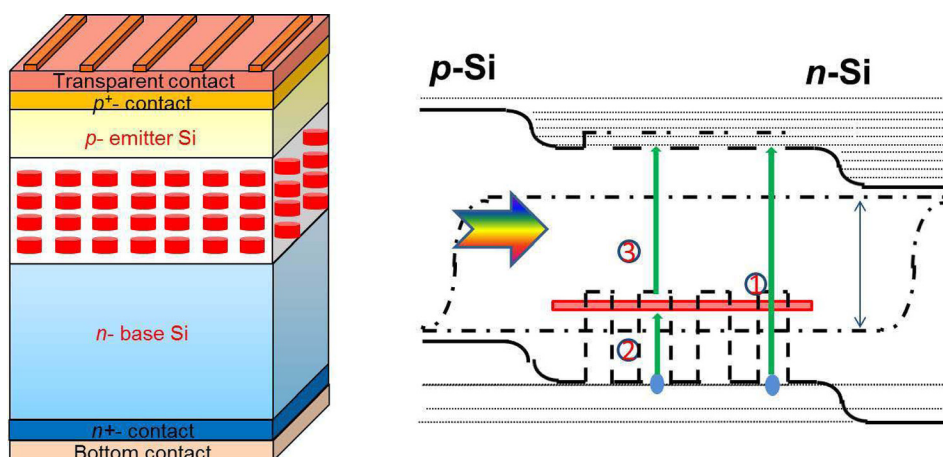

FIG. 2. The explored Ge/Si IBSC's device structure and the corresponding band profile for potential solar cell applications.
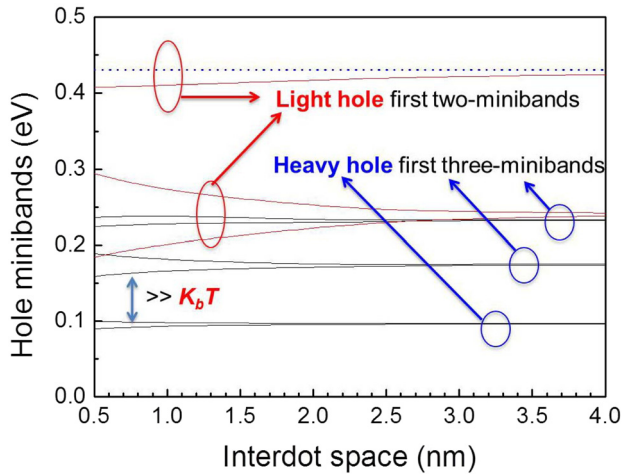
FIG. 3. The miniband formations in the studied Ge/Si QD superlattice, where the diameter $= 6.4$ nm and the thickness $= 4$ nm.

FIG. 5. Plot of conversion efficiency as a function of concentration time. The proposed structure possesses the improved conversion efficiency compared with the conventional one.

9.7 meV to 0.5 meV. To maintain formed miniband rather degraded quantum level, the interdot space should be kept smaller than some value, such as 4 nm. In our recent experiments, a 2.3 nm interdot space has been achieved in various QD superlattices.[7,14]

With the detailed balance model, we calculate the I-V profile of IBSC consisted of Ge QDs with the 6.4 nm diameter, 4 nm thickness, and 2.3 nm interdot space embedded into the crystal silicon matrix. 6000 K blackbody is used to simulate sun illumination. The result is shown in Fig. 4. Under 1 sun illumination, the device exhibits 78 mA/cm^2 short circuit current, 0.74 V open-circuit voltage, and 28.6% conversion efficiency. This efficiency does not remarkably exceed the traditional silicon solar cell. The main reason lies on the silicon's bandgap which is only 1.1 eV, related to the infrared spectrum. Most photons have been absorbed and main energy loss comes from the thermal loss aroused from the small bandgap.

However, under the concentration application, the conversion efficiency of IBSC exhibits a relatively larger enhancement. As shown in Fig. 5, under 200 times concentration, the conversion efficiency of IBSC rapidly increases
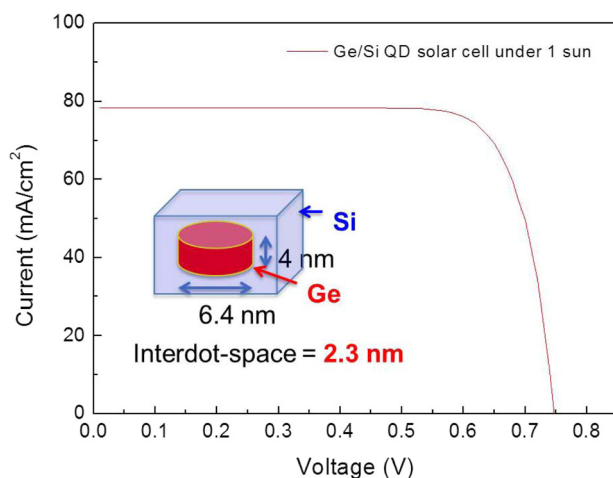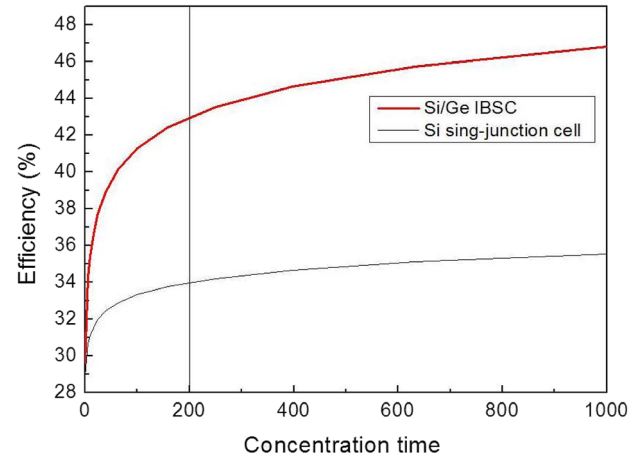
to 42.9%, much higher than the traditional silicon solar cell. Under concentration illuminations, the open-circuit photovoltage gradually approaches to the material bandgap. In addition, the two-photon-transition in IBSC can be viewed as two cascaded sub-cells. Thus, it can gain more enhancement of efficiency than a traditional one. In fact, this special property has also been reported with using a prototype of IBSC.[15] The concentration application is an important consideration in the present energy device technology.

Our top-down process offers a special flexibility on quantum engineering, various matrix materials, which indicates a possibility for optimizing 1 sun application. Some experiments have proved that with H-passivation treatment, amorphous Si bandgap can be nearly linearly controlled from 1.5 to 2.1 eV with increasing H concentration.[16] Figure 6 shows the conversion efficiency of IBSC consists of Ge QD superlattice with various matrix materials. The efficiency can be effectively tuned with various matrices, and the maximum efficiency

FIG. 4. The simulated I-V profile of the Ge/Si IBSC under 1 sun illumination.
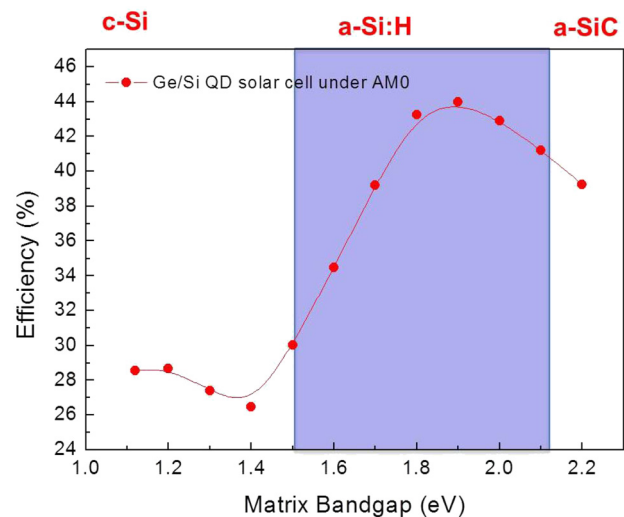

FIG. 6. The conversion efficiency under 1 sun as a function of the matrix bandgap. With H-passivation treatment, amorphous Si bandgap would gradually increase from 1.5 to 2.1 eV; and thus, the conversion efficiency approaches to 44%.

reaches 44.0% under 1 sun, which is related to amorphous Si with 1.9 eV bandgap. This high conversion efficiency sweeps the S-Q limit hinder on Si-based solar cell.

In conclusion, we have studied the intermediate band formation condition and corresponding parameters of the type II Ge/Si QD superlattice. Furthermore, by using the crystalline silicon as the matrix, the IBSC may not be suitable for 1 sun application, but it is a great value under concentration application. By considering an appropriate H-passivation treatment on amorphous Si, the type II Ge/Si IBSC can achieve 44.0% conversion efficiency under 1 sun application. These applications greatly broaden silicon-based solar cell further commercial applications.

[1] M. A. Green, K. Emery, Y. Hishikawa, W. Warta, and E. D. Dunlop, Prog. Photovoltaics **20**, 606–614 (2012).

[2] A. Luque, A. Martí, and C. Stanley, Nat. Photonics **6**, 146–152 (2012).

[3] A. Luque and A. Martí, Phys. Rev. Lett. **78**, 5014–5017 (1997).

[4] A. Martí, E. Antolín, C. R. Stanley, C. D. Farmer, N. López, P. Díaz, E. Cánovas, P. G. Linares, and A. Luque, Phys. Rev. Lett. **97**, 247701(24) (2006).

[5] Y. Okada, T. Morioka, K. Yoshida, R. Oshima, Y. Shoji, T. Inoue, and T. Kita, J. Appl. Phys. **109**, 024301(2) (2011).

[6] A. M. Kechiantz, L. M. Kocharyan, and H. M. Kechiyants, Nanotechnology **18**, 405401(40) (2007).

[7] M. F. Budiman, W. Hu, M. Igarashi, R. Tsukamoto, T. Isoda, K. M. Itoh, I. Yamashita, A. Murayama, Y. Okada, and S. Samukawa, Nanotechnology **23**, 065302(6) (2012).

[8] Y. Li, O. Voskoboynikov, C. P. Lee, S. M. Sze, and O. Tretyak, J. Appl. Phys. **90**, 6416 (2001).

[9] W. G. Hu, T. Inoue, O. Kojima, and T. Kita, Appl. Phys. Lett. **97**, 193106(19) (2010).

[10] A. Lin and J. Phillips, IEEE Trans. Electron Devices **56**, 3168–3174 (2009).

[11] K. Yoshida, Y. Okada, and N. Sano, Appl. Phys. Lett. **97**, 133503(13) (2010).

[12] W. Hu, Y. Harada, A. Hasegawa, T. Inoue, O. Kojima, and T. Kita, Prog. Photovoltaics **21**, 472–480 (2013).

[13] M. Sugiyama, Y. Wang, H. Fujii, H. Sodabanlu, K. Watanabe, and Y. Nakano, J. Phys. D **46**, 024001 (2013).

[14] W. Hu, M. Igarashi, M.-Y. Lee, Y. Li, and S. Samukawa, Nanotechnology **24**, 265401 (2013).

[15] T. Tayagaki, N. Usami, W. Pan, Y. Hoshi, K. Ooi, and Y. Kanemitsu, Appl. Phys. Lett. **101**, 133905(13) (2012).

[16] W. Futako, K. Yoshino, C. M. Fortmann, and I. Shimizu, J. Appl. Phys. **85**, 812 (1999).

[17] J. G. Fossum, R. P. Mertens, D. S. Lee, and J. F. Nijs, Solid-State Electron. **26**, 569 (1983).

[18] L. Löfgren, J. Appl. Phys. **29**, 158 (1958).

[19] O. L. Lazarenkova and A. A. Balandin, J. Appl. Phys. **89**, 5509 (2001).

[20] E. Cassan, J. Appl. Phys. **87**, 7931 (2000).

[21] S. M. Sze, *Physics of Semiconductor Devices* (John Wiley & Sons, New York, 1981), p. 850.